Intercalation of decanoate anions (C10) in layered double hydroxide Mg Al and its application as controlled-release corrosion inhibitor of steel

A. Aitaghzzaf, Y. Zarki, B. Rhouta, A. Khalil, Delphine Veys-Renaux, H. Majdoub, Emmanuel Rocca

Intercalation of decanoate anions (C10) in layered double hydroxide Mg–Al and its application as controlled-release corrosion inhibitor of steel

A. AitAghzzaf [a,*], Y. Zarki [a,d], B. Rhouta [b], A. Khalil [b], D. Veys-Renaux [c], H. Majdoub [a,d], E. Rocca [c]

[a] Nanomaterials, Technology and Innovation Group, ENS, Abdelmalek Essaadi University, Tetouan, Morocco

[b] Laboratoire des Mat´eriaux Innovants, Energie et D´eveloppement Durable, FSTG, Cadi Ayyad University, Marrakech, Morocco

[c] Institut Jean Lamour CNRS-Universit´e de Lorraine, Dept CP2S, BP 70239, 54506 Vandoeuvre-Les-Nancy, France

[d] IMED-Lab, FS, Abdelmalek Essaadi University, Tetouan, Morocco

* Corresponding author. E-mail address: a.aitaghzzaf@uae.ac.ma (A. AitAghzzaf).

Keywords: LDH; Decanoate; Pigment; Paint; Inhibition; Steel ; EIS

ABSTRACT

This study focuses on the preparation and characterization of a novel anticorrosion pigment based on decanoate anions (C_{10}^-) intercalated within layered double hydroxide (LDH) Mg–Al. The LDH-NO3, LDH-C_{10} were synthesized by a simple co-precipitation method and analyzed by XRD, infrared spectroscopy, thermogravimetry and electronic microscopy. The LDH-C10 pigment with a basal distance of about 20 Å was consistent with the arrangement of C_{10} anions in bilayer. The inhibition efficiency of the LDH-C_{10} pigment in electrolyte and in alkyd resin paint was studied by electrochemical impedance spectroscopy and potentiodynamic techniques. The pigments act as a C_{10}^- nanocontainer, which release the C_{10}^- anions in contact with chloride ions that lead to the formation of a passive layer on steel. In alkyd resin, the LDH-C_{10}-enriched organic coating exhibit very interesting anticorrosive performance in NaCl electrolyte during 40 days of immersion.

1. Introduction

To prevent the corrosion of metallic materials in industrial and/or marine atmospheric conditions, the organic coatings are the most widespread approach. The organic polymer coatings develop an effective barrier against corrosive species and can be easily enriched in different additives such as anticorrosive pigments. Since several ten years ago, researches were

focused on the replacement of chromatesbased pigments because of their toxicity and carcinogenic effects [1]. Nowadays, the Cr(VI)-based compounds have been substituted by compounds based on zinc or aluminum phosphate, which are today present in many commercial paint formulation to protect steels [2–4]. However, the dissemination of phosphate anions and heavy metal cations in the environment begins to be regulated and controlled [4,5]. Consequently, the next generation of anticorrosive pigments should be without soluble phosphate and metallic cations. In addition, like the Cr (VI) based compounds, the phosphate-based compounds are soluble anticorrosion pigments which induce the formation of holes or voids in the polymer film during the life cycle of the coating. The exchangeable materials like clay minerals [6–8] or insoluble zirconium phosphate (ZrP) [9] constitute some interesting alternatives, whose the release mechanism of the corrosion inhibitor is based on an exchange reaction. Especially, the anionic clay family named layered double hydroxide (LDH), have been widely used as reservoir of anions due to their doublelayered structure and their important anion exchange capacity [10–12]. They have already been developed and studied for the controlled release of drug molecules in medicine and phytosanitary compounds [13–15] or the design of new materials [16]. In the field of the corrosion protection, some studies have been carried out to develop Cr(VI)-free anticorrosive pigments based on LDH intercalated with oxometallate anions such as molybdate [17,18], vanadate [19] or organic inhibitor such as mercapto-azol-type molecules [20,21]. Nevertheless, many azol-type molecules are toxic for the environment and should be avoided. Thus, the use of non-toxic and not-regulated compounds should be prioritized in the development of new anticorrosive pigments.

In this framework, certain carboxylic acids with linear carbon chains have been shown to be excellent corrosion inhibitors for various metals including copper, zinc, iron, magnesium alloys, and lead. The effectiveness of these carboxylic acids is attributed to their ability to form insoluble metallic soaps on the metal surface [22–25]. The decanoate anion ($CH_3(CH_2)_8COO^-$ noted C_{10}^-) has been investigated on a variety of metallic substrates and presents a good compromise between its solubility in water and the insolubility of the corresponding metallic carboxylate compound that can be formed on metallic surfaces [26,27].

The objective of the article is to propose a new generation of anticorrosion pigment without any environmentally-regulated compounds, with a simple one-pot synthesis process and with an anticorrosion mechanism based on an exchange reaction. For that, the preparation of LDH intercalated with nitrate and decanoate anions by direct coprecipitation process was described at room temperature and pressure. The new pigments were analyzed by XRD, FTIR

spectroscopy and thermogravimetry to describe their chemical composition and crystallographic structure. The particle size of these pigments was evaluated by electronic microscopy. The properties and anticorrosion efficiency of LDH-C_{10} were compared to a simple LDH compound intercalated with nitrate (LDH-NO_3).

Afterwards, the anticorrosive properties of the different elaborated LDH pigments were studied by stationary technique such as potentiodynamic and transient technique EIS upon their addition to NaCl corrosive medium and their incorporation in an organic coating on steel as well.

2. Materials and methods

2.1. Preparation

The solution of sodium decanoate ($CH_3(CH_2)_8COONa$ noted NaC_{10}) was prepared by acid-base reaction between decanoic acid (CH3(CH2)8COOH noted HC10) and sodium hydroxide NaOH. LDH-NO_3 and LDH-C_{10}, were prepared by a direct co-precipitation process, also named one-pot process. Firstly, the solution of anions was placing a three-neck flask at pH = 9 under stirring at 50°C. In the studied case, 50 mL of 0.5 mol/L $NaNO_3$ or NaC_{10} solution was used. Then a solution of metal salts was progressively added at 0.06 mL/min to the solutions of anions at pH = 9 to directly form the intercalated layered double hydroxide. The Mg–Al LDH was precipitated by adding 100 mL of 0.5 mol/L $Mg(NO_3)_2{\cdot}6H_2O$ and 0.25 mol/L $Al(NO_3)_3{\cdot}9H_2O$ solutions. During the reaction time, the pH solution was maintained to 9 by adding a 2 mol/L NaOH solution and the reaction environment was controlled under N_2 to prevent the adsorption of CO_2 and the formation of carbonated LDH. The resulting white product was centrifuged at 4200 rpm, washed tree times with distilled water and dried at 80 ◦C for 10 h.

2.2. Characterization techniques

The LDH-NO_3 and LDH-C_{10} samples were characterized by XRD using Philips XPert Pro diffractometer with copper anticathode ($\lambda K\alpha_1$ = 1.54056 Å). X-ray diffraction patterns were recorded for 2θ ranging from 3◦ to 40◦ with steps of 0.02. FTIR analysis was carried out with a BRUKER IFS 55 equipped with a broadband detector. The acquisition was performed in the frequency range of 400 to 4000 cm^{-1}. Microstructural characterization and elemental analysis

of the samples were carried out by Field Emission Scanning Electron Microscopy (FE-SEM JEOLJ7600F) equipped with Energy Dispersion Spectrometer (EDS).

2.3. Electrochemical studies

Two samples of mild steel, of surfaces 2.27 cm^2 and 36 cm^2 each one, were used as working electrodes. Their surfaces were prepared by polishing using successively silicon carbide (SiC) abrasive papers of grades 120, 400, and 2500. After that, metallic substrate surface was washed with ethanol, hair-dried and stored for subsequent use. To perform electrochemical test, the classical three electrodes cell was used. The horizontal working electrode was faced to a platinum grid used as counter electrode while KCl-saturated calomel electrode (SCE) was used as a reference electrode. The steel samples (2.27 cm^2) were immersed in aerated NaCl medium containing 1 $g{\cdot}L^{-1}$ of pigments (LDH-NO_3 or LDHC_{10}).

To prepare the organic coatings, the LDH-C_{10} and LDH-NO_3 pigments were mechanically dispersed in a pure alkyd resin at 5 wt% with a propeller shaker at 600 rpm for 30 min. The so loaded alkyd resin was thereafter spread onto metallic substrate using a bar coater to form a coating of about 100 μm of thickness. The coated samples ware afterwards air-dried for three days. The electrochemical impedance tests on painted steel were carried out in aerated 3 wt% NaCl electrolyte.

The electrochemical measurements were carried out by using a potentiostat Gamry 3000 monitored with software Gamry. Corrosion evaluations were achieved by measuring first the corrosion potential and thereafter the electrochemical impedance spectrum from 100 kHz to

10 mHz with a 10 mV amplitude at open-circuit potential. The cathodic and anodic potentiodynamic curves were performed in two different experiments after 20 h of immersion in NaCl 0.1 M, from the open-circuit potential EOC to EOC-250 mV and from EOC to EOC + 500 mV with a sweep rate of 1 mV/s.

The repeatability of electrochemical measurements was verified by performing 3 tests on each sample. The error measurement can be estimate to about 10–15 %. The treatment of EIS data was carried out using the ZSimpWin software [25].

3. Results and discussion

3.1. Characterizations of LDH-pigments

Powder XRD patterns recorded on samples LDH-NO_3 and LDH-C_{10} are shown in Fig. 1. They showed reflections characteristic of LDH compounds whose angular positions and hence corresponding reticular distances depend on the nature of charge compensating anion. Indeed, LDH-NO_3 diffractogram showed a series of the main reflection (003) at 2θ around 10◦ along with its corresponding harmonics (006) and (009) at 20 and 30◦ respectively corresponding to basal distance at 8.8 Å along with 4.4 and 2.9 Å respectively. As far as LDH-C_{10} is concerned, the corresponding XRD pattern revealed the detection of the main basal reflection (003) at almost 3◦ in 2θ corresponding to a basal distance of around 29.6 Å while its harmonic peaks (006) and (009) were observed at 2θ about 6 and 9◦ corresponding to reticular distances around 14.8 and 9.9 Å respectively. It is worth noting that the basal distance d_{003} shifted from 8.8 Å for LDH-NO_3 to 29.6 Å for LDH-C_{10}, i.e. an increase of about 20.8 Å. Knowing that hydrotalcite-like hydroxide layers of LDH are negatively charged so that they are neutrally compensated by anions placed in interlayer spaces. Therefore, the beforehand mentioned increase in d_{003} is likely ascribed to the huge size of C10 anions with respect to that of NO_3^- ones leading to a consequent greater expansion of LDH interlayer spaces due to their occupancy by C10 entities in comparison with NO_3^- species. This result ascertained the successful intercalation of the decanoate anions within LDH galeries.

Taking into account the thickness 2.5 Å of C_{10} anions, these later cannot be lied inside LDH interlayer spaces in the form of mono or bi or pseudo-trilayers. Nevertheless, the increase magnitude order (≈ 20.8 Å) assessed above may be rather in agreement with the arrangement of the decanoate anions ($C_9H_{19}COO^-$) in the form a paraffinic bilayer schematized in the Fig. 2. In fact, the theoretical basal layer spacing (d_{003}) for a bilayer arrangement can be evaluated by using the following relation [28]:

$d_{003} = 0.254 \sin\alpha\ (n - 1) + 2d_0 + d_1 + d_2$,

d_0: distance between the ionized head of the carboxylate anions and the metal hydroxide layers estimated as 0.14 nm [29];d_1: thickness of the brucite $Mg(OH_2$ -like metal layers (0.48 nm) [30];d_2: distance between two terminal CH3 groups approximately 0.3 nm [31].

In this case, starting from the d_{003} value (≈ 29.6 Å) beforehand assessed for LDH-C10, the tilt angle α between the C_{10} alkyl chain and the metal hydroxide layers can be evaluated to about 60◦, which is consistent with previous works on the intercalation of linear alkyl sulfate in LDH [28–31].

The FTIR spectra of the LDH-NO_3 and LDH-C_{10}, displayed in the Fig. 3, further confirm the chemical structure of the samples. The broad absorption band ranging from 3000 to 3600 cm^{-1} observed in both the samples is obviously ascribed to the stretching modes of OH groups in the metal hydroxide sheets and water molecules inside the interlamellar space [32]. The corresponding HOH bending vibrations of H_2O were detected at 1625 cm^{-1}. In the low frequency region (500 to 900 cm^{-1}), the spectra reveal also the characteristic stretching bands of Al-OH and Mg-OH groups named lattice vibrations of the hydrotalcite sheets, already reported by Kloprogge et al. [33]. Additionally, the LDH-NO_3 spectrum exhibited two fingerprints peaks at 1384 cm^{-1} and 1040 cm^{-1}, attributed to the NO stretching vibrations of NO_3^- anions [32].

Regarding LDH-C_{10} material, it should be noted the observation of several absorption bands characteristic of decanoate species. Indeed, the bands at 1580 and 1400 cm^{-1} are ascribable to the symmetric and antisymmetric stretching vibrations of the COO^-groups of decanoate anions. Likewise, the characteristic CH2 stretching vibrations of the carbon chain of decanoate were observed at 2960, 2920 and 2860 cm^{-1}.

The thermal decomposition of LDH-NO_3 and LDH-C_{10} samples are displayed in Fig. 3. The thermogravimetric measurements of LDH-NO_3 show two main mass losses. The first one from 50°C to 200°C, appearing doubled, is attributed to the removal of about 5 wt% of physically adsorbed water between 50°C and 100°C whereas the second one corresponded to the loss of almost 10 wt% of interlamellar water in the range of [100°C–200°C)] as shown in the Fig. 3a. Afterwards, the second loss of about 40 wt% observed between 300 and 600°C is likely due to the removal of structural OH groups (dehydroxylation) along with the decomposition of NO3□ anions. The decomposition reaction of LDH-NO_3 can occur as follows:

$$Mg_{1-x}Al_x(OH)_2(NO_3)_x, zH_2O \rightarrow (x/2)\ Mg_2O_4 + (1 - 3x/2)\ MgO + x\ NO_2 + (x/4)\ NO_2 + (1+z)H_2O.$$

Considering the different corresponding losses cited above, x and z values can be evaluated to be about 0.33 and 0.5 respectively, so that the chemical composition of LDH-NO3 can be formulated as: $Mg_{0.67}Al_{0.33}(OH)_2(NO_3)_{0.33}, 0.5H_2O$.

On the other hand, the thermal decomposition of LDH-C_{10} sample also exhibits two main mass losses evidenced in Fig. 3b. The first one, of about 5 wt% occurring around 100 ◦C, can be similarly attributed to the removal of surface adsorbed water, while the release of almost 7 wt%

interlamellar water can occur until 200°C. Between 200°C and 600°C, the second main mass losses can be clearly ascribed to the decomposition of decanoate anions and the removal of hydroxyl group in the interlayer spaces. According to the TG analysis results (Fig. 4), x and z values can be determined in the same way than above in that chemical composition formulae of LDH-C_{10} can be expressed as: $Mg_{0.67}Al_{0.33}(OH)_2(C_{10})_{0.33}\cdot 0.5H_2O$.

The SEM micrographs of LDH-NO_3 and LDH-C_{10} powders, shown in Fig. 5, reveal the morphology of corresponding particles. Both the samples have the typical plate-like morphology characteristic of lamellar materials in general and LDH in particular. The particles size of both samples is relatively small, ranging from 50 nm to 200 nm.

3.2. Electrochemical measurements of steel in NaCl electrolyte containing pigments

The properties of corrosion inhibition of steels were first evaluated in NaCl electrolyte on steel. EIS measurements were performed after 20 h of immersion in 0.1 M NaCl solution without and with a dispersion of LDH-NO_3 and LDH-C_{10}. The Bode spectra of EIS data and the equivalents circuits models are displayed in the Fig. 6.

Without pigments or with LDH-NO_3 powder, the shape of the impedance spectra recorded in NaCl solution shows a single relaxation phenomenon with a characteristic frequency of around 5 Hz (Fig. 6). The equivalent circuit is consisting of the electrolyte resistance (Re), the high frequency resistance (RHF), assigned to the resistance of corrosion products layer and the charge transfer resistance, and the constant phase element (CPE defined by QHF, n) with a n factor around 0.8, assigned to the double layer capacitance of the steel/electrolyte interface. The impedance of CPE, defined as $ZCPE = (Q \times (j\omega)^n)^{-1}$, is used to take into account the surface heterogeneities.

Table 1 gathers the data deduced from simulation with ZSimpWin software. Table 1 shows that without pigment the RHF value is low, around 2120 $\Omega\cdot cm^2$ and the QLF value is relatively high, around 185 $\mu S\ s^n\ cm^{-2}$ because the corrosion layer is very porous, partially conductive, inducing a large electroactive surface, as observed by SEM observations in the Fig. 7a [34].

The presence of the LDH-NO_3 pigment slightly enhances the RHF value and reduces the QHF value, compared to the sample without pigments (3600 $\Omega\cdot cm^2$ and 157 $\mu S\cdot s^n\cdot cm^{-2}$). This small resistance increase can be due to the deposition of LDH mineral particles on the electrode

surface and the small corrosion inhibiting effect of NO_3^- ions [35]. In fact, nitrate ions can be released by ionic exchange with chloride according to the reaction:

$Mg_{0.67}Al_{0.33}(OH)_2(NO_3)_{0.33} + 0.33\ Cl^- \rightarrow Mg_{0.67}Al_{0.33}(OH)_2(Cl^-)_{0.33} + 0.33\ NO_3^-$.

As observed in the Fig. 7b, the presence of nitrate slightly changes the formation and crystallization of the corrosion products on steel, which explains the increase of RHF until 3600 $\Omega \cdot cm^2$ in the Table 1. Actually, the oxidant property of nitrate ions leads an improvement and reinforcement of the natural corrosion product layer in steel.

In presence of the LDH-C_{10}, the impedance diagram, displayed in the Fig. 6b clearly reveals two relaxation phenomena: the first one at low frequency at 0.3 Hz (RLF, QLF) and the second one at high frequency around 300 Hz (RHF, QHF) (Fig. 6b). The high frequency relaxation phenomenon is assigned to the charge transfer resistance at the electrochemical interface and the double layer capacitance. The RHF resistance value with LDH-C10 has the same order of magnitude than the one without pigment or with LDH-NO_3. Nevertheless, the decrease of QHF reveals the absence of the porous corrosion products layer. In addition, no rust-colored corrosion products were observed on the surface after the 24 h immersion test with LDH-C_{10}. At low frequency, the dielectric phenomenon can be attributed to an ionic diffusion across an outer layer, as proven by the n value closed to 0.5. According to previous studies, Mirambet et al. [36] have clearly shown that in presence of a high concentration of decanoate anions, a protective layer in the form of platelets of crystallized iron carboxylate compound can be formed on the electrode surface. In our case, a dense and compact passive layer, enriched in carbon according to EDS analysis (not reported), can be observed on the surface of steel in contact with LDH-C_{10}, as exhibited by the Fig. 7c. Nevertheless, the C_{10}-enriched protective layer appears to be very poorly crystallized, because decanoate anions are only provided by the ionic exchange reaction of LDH with chloride, as follows:

$Mg_{0.67}Al_{0.33}(OH)_2(C_{10})_{0.33} + 0.33\ Cl^- \rightarrow Mg_{0.67}Al_{0.33}(OH)_2(Cl^-).33 + 0.33\ C_{10}^-$.

Subsequently, a precipitation reaction occurs upon contact with Fe^{3+} cations, resulting in the formation of a passive layer composed of iron carboxylate. This precipitation reaction occurs when the solubility product is reached [36]:

$Fe^{3+} + 3C_{10}^- \rightarrow Fe(C_{10})_3$.

After 20 h of immersion in 0.1 M NaCl, the potentiodynamic plots in Fig. 8 confirm the corrosion-inhibitor behavior of LDH pigments on mild steel. These polarization curves revealed

a decrease of the corrosion current density of steel in presence of LDH. With LDH-NO_3, the anodic current density is poorly reduced compared to the one without pigment, whereas the cathodic current density due to the oxygen reduction is clearly diminished, which explain the slight shift of the corrosion potential around -740 mV. This low inhibition of the cathodic kinetic can be explained by the barrier effect of the stacking of the LDH powder on the steel surface. In presence of LDH-C10, the corrosion current density is by a ten-factor because the anodic current density is greatly reduced, in addition to the decrease of the current density. Consequently, the anodic curve shows a large passivation plateau with a passive current at around 10 $\mu A \cdot cm^{-2}$. The LDH-C_{10} pigment show both a cathodic inhibition and an anodic inhibition, which is explained by the presence of an outer layer observed by SEM and detected by EIS.

3.3. Electrochemical measurements of steel coated with LDH-enriched alkyd resin in NaCl

The protection behavior of the corrosion inhibitor pigments was evaluated in an alkyd-type organic coating on steel in a corrosive electrolyte containing 3 wt% NaCl. The pigment content in the alkyd resin is 5 wt% and the thickness of the dry coatings is around to 80 ± 0.5 μm. The LDH pigments are homogeneously dispersed over the entire thickness of the coating, but they form some clusters of about 1 μm in the polymer (Fig. 9).

The EIS measurements were carried out for 40 days in 3 % wt. NaCl. The Fig. 10 shows the Bode plots of the EIS data, obtained on the coated steel samples after immersion in 3 wt% NaCl at different immersion times.

In the pigment-free alkyd coating, a significant drop in values of impedance modulus at low frequencies was observed after 20 days of immersion. These low values are the results of the delamination of the coating and the formation of corrosion products, as revealed by the direct observation of the surface after the immersion after 40 days of immersion. On the other hand, until 20 days of immersion, the electrochemical interface exhibits a capacitive behavior at high frequency (104 to 105 Hz) with a high phase (between 60 and 80◦), which indicate a good structural integrity of the metal/organic coating interface [37]. After 20 days, the organic coating is rapidly damaged. The evaluation of the corrosion protection of organic coating can be also assessed by plotting the impedance modulus at 10 mHz (|Z|10mHz) versus the immersion time, as shown in Fig. 11 [37–40].

For alkyd coatings enriched into each of both the types of LDH, the impedance modulus at low frequency remains constant at high value around $5 \cdot 10^6$ Ω cm^2 for the 40 days of immersion. Simultaneously, the phase shift at high frequency remains at a high value between 60 and 80°, which suggest that the capacitive behavior of the electrochemical interface seems to be poorly affected upon the ageing in the NaCl electrolyte. Nevertheless, for the LDH-NO_3 pigment, a beginning of degradation can be observed by the decrease of the impedance modulus and a decrease of the phase shift starting from around 10^2 Hz in the EIS spectrum at 40 days of immersion. Concerning organic revetment incorporating the LDH-C_{10} pigment, it can be seen a very interesting corrosion protection performance after 40 days of immersion.

These findings indicate that incorporating LDH-C_{10} into alkyd paint is a successful approach to enhance its anti-corrosive properties. Additionally, they suggest that this modification leads to a sustained inhibiting effect over a prolonged duration when compared to a pure alkyd coating. This effect is probably related to a continuous release of decanoate from LDH-C_{10}. Actually, the aggressive chloride ions may come into contact with dispersed LDH, which leads to the entrapment of This process effectively reduces the concentration of aggressive ions in the local environment in the coating. This may provide a sustained inhibiting effect, leading to improved corrosion resistance over time. These results are promising for the development of more effective anticorrosion coatings and provide valuable insight into the mechanisms underlying their performance.

4. Conclusion

Mg–Al layered double hydroxide (LDH), loaded with decanoate anions, has been successfully synthesized using a direct coprecipitation process (one-pot process) at room temperature and pressure with a particle size at a 100 nm-scale. Decanoate anions (C_{10}^-) is intercalated in a tilted double layer into the interlamellar space of double layer hydroxide, according to the chemical formulae: $Mg_{0.67}Al_{0.33}(OH)_2(C_{10})_{0.33} \cdot 0.5H_2O$.

The intercalated LDH acts as a nanocontainer of corrosion inhibitor and releases the decanoate anions by ionic exchange in NaCl solution while the corrosive chloride ions are inserted in the structure. The EIS study of steel in presence of LDH-C_{10} and surface analysis confirm the formation of a C_{10}-enriched passive layer, which reveal an efficient corrosion protection ability. All these results were further corroborated by the potentiodynamic measurements. In alkyd resin, the LDH-C_{10} pigments allow to maintain the structural integrity of the organic coating by

inhibiting the delamination during 40 days of immersion in NaCl corrosive medium. By comparing with LDH-NO_3, the nanometer platelets of LDH matrix does not contribute directly to the corrosion inhibition process. Nevertheless, the platelets reinforce the barrier effect of the polymer coating and contribute to maintain a high impedance and a good protection of the alkyd polymer film after long immersion in NaCl.

This study has shown the feasibility of developing nanocontainers of corrosion inhibitor based on double layer hydroxide to formulate protective organic coatings without phosphate and heavy metal ions such as Zn^{2+}. Particularly, the LDH-C_{10} can provide prolonged and smart release of the inhibiting species on demand via an exchange mechanism with the corrosive anions as chlorides or sulfates. It could be an adequate anticorrosion pigment based on a low cost and environment friendly preparation process.

CRediT authorship contribution statement

A. AitAghzzaf: Writing – original draft, Methodology, Formal analysis, Conceptualization.

Y. Zarki: Writing – original draft, Visualization.

B. Rhouta: Visualization, Validation.

A. Khalil: Visualization.

D. Veys-Renaux: Writing – review & editing, Visualization, Resources.

H. Majdoub: Writing – review & editing, Visualization.

E. Rocca: Writing – review & editing, Validation, Methodology, Formal analysis.

Declaration of competing interest

We wish to confirm that there are no known conflicts of interest associated with this publication and there has been no significant financial support for this work that could have influenced its outcome.

References

[1] M. Costa, Toxicity and carcinogenicity of Cr(VI) in animal models and humans, Crit. Rev. Toxicol. 27 (5) (1997) 431–442.

[2] C. Dey´a, G. Blustein, B. del Amo, R. Romagnoli, Evaluation of eco-friendly anticorrosive pigments for paints in service conditions, Prog. Org. Coat. 69 (1) (2010) 1–6.

[3] R. Naderi, M.M. Attar, The role of zinc aluminum phosphate anticorrosive pigment in protective performance and cathodic disbondment of epoxy coating, Corros. Sci. 52 (4) (2010) 1291–1296.

[4] V. Ishchenko, Environment contamination with heavy metals contained in waste, Environ. Prob. 3 (1) (2018) 21–24.

[5] N. Singh, Andrew Turner, Trace metals in antifouling paint particles and their heterogeneous contamination of coastal sediments, Mar. Pollut. Bull. 58 (4) (2009) 559–564.

[6] N. Granizo, J.M. Vega, D. de la Fuente, J. Simancas, M. Morcillo, Ion-exchange pigments in primer paints for anticorrosive protection of steel in atmospheric service: cation-exchange pigments, Prog. Org. Coat. 75 (2012) 147–161.

[7] A. Ait Aghzzaf, B. Rhouta, E. Rocca, A. Khalil, J. Steinmetz, Corrosion inhibition of zinc by calcium exchanged beidellite clay mineral: a new smart corrosion inhibitor, Corros. Sci. 80 (2014) 46–52.

[8] A. Ait Aghzzaf, B. Rhouta, J. Steinmetz, E. Rocca, L. Aranda, A. Khalil, J. Yvon, L. Daoudi, Corrosion inhibitors based on chitosan-heptanoate modified beidellite, Appl. Clay Sci. 65–66 (2012) 173–178.

[9] I. Bouali, E. Rocca, D. Veys-Renaux, B. Rhouta, A. Khalil, A. Aït Aghzzaf, Ca2+- exchange in layered zirconium orthophosphate, α-ZrP: chemical study and potential application for zinc corrosion inhibition, Appl. Surf. Sci. 422 (2017) 778–786.

[10] M. Zheludkevich, S.K. Poznyak, L.M. Rodrigues, D. Raps, T. Hack, L.F. Dick, Active protection coatings with layered double hydroxide nanocontainers of corrosion inhibitor, Corros. Sci. 52 (2) (2010) 602–611.

[11] Y. Wang, D. Zhang, Synthesis, characterization, and controlled release anticorrosion behavior of benzoate intercalated Zn–Al layered double hydroxides, Mater. Res. Bull. 46 (2011) 1963–1968.

[12] T.T.X. Hang, T.A. Truc, N.T. Duong, N. P´eb`ere, M.G. Olivier, Layered double hydroxides as containers of inhibitors in organic coatings for corrosion protection of carbon steel, Prog. Org. Coat. 74 (2012) 343–348.

[13] A.I. Khan, A. Ragavan, B. Fong, C. Markland, M. O'Brien, T.G. Dunbar, G. R. Williams, D. O'Hare, Recent developments in the use of layered double hydroxides as host materials for the storage and triggered release of functional anions, Ind. Eng. Chem. Res. 48 (2009) 10196–10205.

[14] H. Nakayama, H. Akasaka, M. Tsuhako, Complete protection of sodium valproate from humidity by using a hydrotalcite composite, J. Pharm. Sci. 98 (2009) 46–49.

[15] F.S. Li, L. Jin, J.B. Han, M. Wei, C.J. Li, Synthesis and controlled release properties of prednisone intercalated Mg–Al layered double hydroxide composite, Ind. Eng. Chem. Res. 48 (2009) 5590–5597.

[16] J. Wang, J.D. Zhou, Z.S. Li, Q. Liu, P.P. Yang, X.Y. Jing, M.L. Zhang, Design of magnetic and fluorescent Mg–Al layered double hydroxides by introducing Fe3O4 nanoparticles and Eu3+ ions for intercalation of glycine, Mater. Res. Bull. 45 (2010) 640–645.

[17] X. Yu, J. Wang, M.L. Zhang, P.P. Yang, L.H. Yang, D.X. Cao, J.Q. Li, One-step synthesis of lamellar molybdate pillared hydrotalcite and its application for AZ31 Mg alloy protection, Solid State Sci. 11 (2009) 376–381.

[18] X. Yu, J. Wang, M.L. Zhang, L.H. Yang, J.Q. Li, P.P. Yang, D.X. Cao, Synthesis, characterization and anticorrosion performance of molybdate pillared hydrotalcite/in situ created ZnO composite as pigment for Mg–Li alloy protection, Surf. Coat. Technol. 203 (2008) 250–255.

[19] R.G. Buchheit, H. Guan, S. Mahajanam, F. Wong, Active corrosion protection and corrosion sensing in chromate-free organic coatings, Prog. Org. Coat. 47 (2003) 174–182.

[20] S.K. Poznyak, L.M. Tedim, A.N. Rodrigues, M.L. Salak, L.F.P. Zheludkevich, M.G. S. Dick, Ferreira, Novel inorganic host layered double hydroxides intercalated with guest organic inhibitors for anticorrosion applications, ACS Appl. Mater. Interfaces 1 (2009) 2353–2362.

[21] M. Kendig, M. Hon, A hydrotalcite-like pigment containing an organic anion corrosion inhibitor, Electrochem. Solid St. 8 (2005) 10–11.

[22] J. Peultier, M. François, J. Steinmetz, Anhydrous polymeric zinc (II) heptanoate, Acta Crystallogr. Sect. C Cryst. Struct. Commun. C55 (1999) 2064–2065.

[23] J. Peultier, E. Rocca, J. Stienmetz, Zinc carboxylating: a new conversion treatment of zinc, Corros. Sci. 45 (2003) 1703–1716.

[24] E. Rocca, C. Rapin, F. Mirambet, Inhibition treatment of the corrosion of lead artefacts in atmospheric conditions and by acetic acid vapour: use of sodium decanoate, Corros. Sci. 46 (2004) 653–665.

[25] E. Rocca, C. Caillet, A. Messbah, M. François, J. Steinmetz, Intercalation in zinclayered hydroxide: zinc hydroxyheptanoate used as protective material on zinc, Chem. Mater. 18 (2006) 6186–6193.

[26] S. Jacques, E. Rocca, M.-J. Stebe, J. Steinmetz, "Carboxylatation" coating on zinc: a chemical conversion in organized molecular systems containing carboxylic acid, Surf. Coat. Technol. 202 (2008) 3878–3885.

[27] A. Aït Aghzzaf, B. Rhouta, E. Rocca, A. Khalil, C. Caillet, R. Hakkou, Heptanoic acid adsorption on grafted palygorskite and its application as controlled-release corrosion inhibitor of steel, Mater. Chem. Phys. 148 (2014) 335–342.

[28] H. Kopka, K. Beneke, G. Lagaly, Anionic surfactants between double metal hydroxide layers, J. Colloid Interface Sci. 123 (2) (1988) 427–488.

[29] T. Itoh, N. Ohta, T. Shichi, T. Yui, K. Takagi, The self-assembling properties of stearate ions in hydrotalcite clay composites, Langmuir 19 (2003) 9120–9126.

[30] A.N. Ay, B.Z. Karan, A. Temel, L. Mafr, Layered double hydroxides with interlayer borate anions: a critical evaluation of synthesis methodology and pH-independent orientations in nano-galleries, Appl. Clay Sci. 51 (2011) 308–316.

[31] M. Meyn, K. Beneke, G. Lagaly, Anion-exchange reactions of layered double hydroxides, Inorg. Chem. 29 (1990) 5201–5207.

[32] K. Nakamoto, Infrared and Raman Spectra of Inorganic and Coordination Compounds: Part A: Theory and Applications in Inorganic Chemistry, Ed Wiley- Blackwell, 2008.

[33] J. Theo Kloprogge, R.L. Frost, Fourier transform infrared and Raman spectroscopic study of the local structure of Mg-, Ni-, and Co-hydrotalcites, J. Solid State Chem. 146 (1999) 506–515.

[34] E. Rocca, H. Faiz, P. Dillmann, D. Neff, F. Mirambet, Electrochemical behavior of thick rust layers on steel artefact: mechanism of corrosion inhibition, Electrochim. Acta 316 (1) (2019) 219–227.

[35] M. Murmu, S.K. Saha, N. Chandra Murmu, P. Banerjee, Chapter 14 — Nitrate as corrosion inhibitor, in: Inorganic Anticorrosive Materials, Past, Present and Future Perspectives, Ed Elsevier, 2022, pp. 269–296.

[36] F. Mirambet, S. Reguer, E. Rocca, A complementary set of electrochemical and Xray synchrotron techniques to determine the passivation mechanism of iron treated in a new corrosion inhibitor solution specifically developed for the preservation of metallic artefacts, Appl. Phys. A 99 (2) (2010) 341–349.

[37] A. Dehghani, M. Zabihi-Gargari, M.T. Majd, Development of a nanocomposite coating with anti-corrosion ability using graphene oxide nanoparticles modified by Echium ammonium extract, Prog. Org. Coat. 166 (2022) 106778.

[38] Y. Mei, J. Xu, L. Jiang, Q. Tan, Enhancing corrosion resistance of epoxy coating on steel reinforcement by aminobenzoate intercalated layered double hydroxides, Prog. Org. Coat. 134 (2019) 288–296.

[39] Y. Su, S. Qiu, D. Yang, S. Liu, H. Zhao, L. Wang, Q. Xue, Active anti-corrosion of epoxy coating by nitrite ions intercalated MgAl LDH, J. Hazard Mater. 391 (2020) 122215.

[40] V.S. Raja, R. Gayathiri Devi, A. Venugopal, N.C. Debnath, J. Giridhar, Evaluation of blistering performance of pigmented and unpigmented alkyd coatings using electrochemical impedance spectroscopy, Surf. Coat. Technol. 107 (1) (1998) 1–11.

Table 1. Values of the equivalent electrical circuit elements calculated from the fitting results of EIS data of Fig. 6.

	R_{HF}/ $\Omega \cdot cm^2$	Q_{HF}/ $\mu S \cdot s^n \cdot cm^{-2}$	n	R_{LF}/ $\Omega \cdot cm^2$	Q_{LF}/ $\mu S \cdot s^n \cdot cm^{-2}$	n
Without inhibitor	2120	185	0.82	/	/	/
LDH-NO_3	3600	157	0.84	/	/	/
LDH-C_{10}	1440	8	0.86	49,000	60	0.57

Fig. 1. XRD patterns of LDH pigments: (a) LDH-NO_3 and (b) LDH-C_{10}

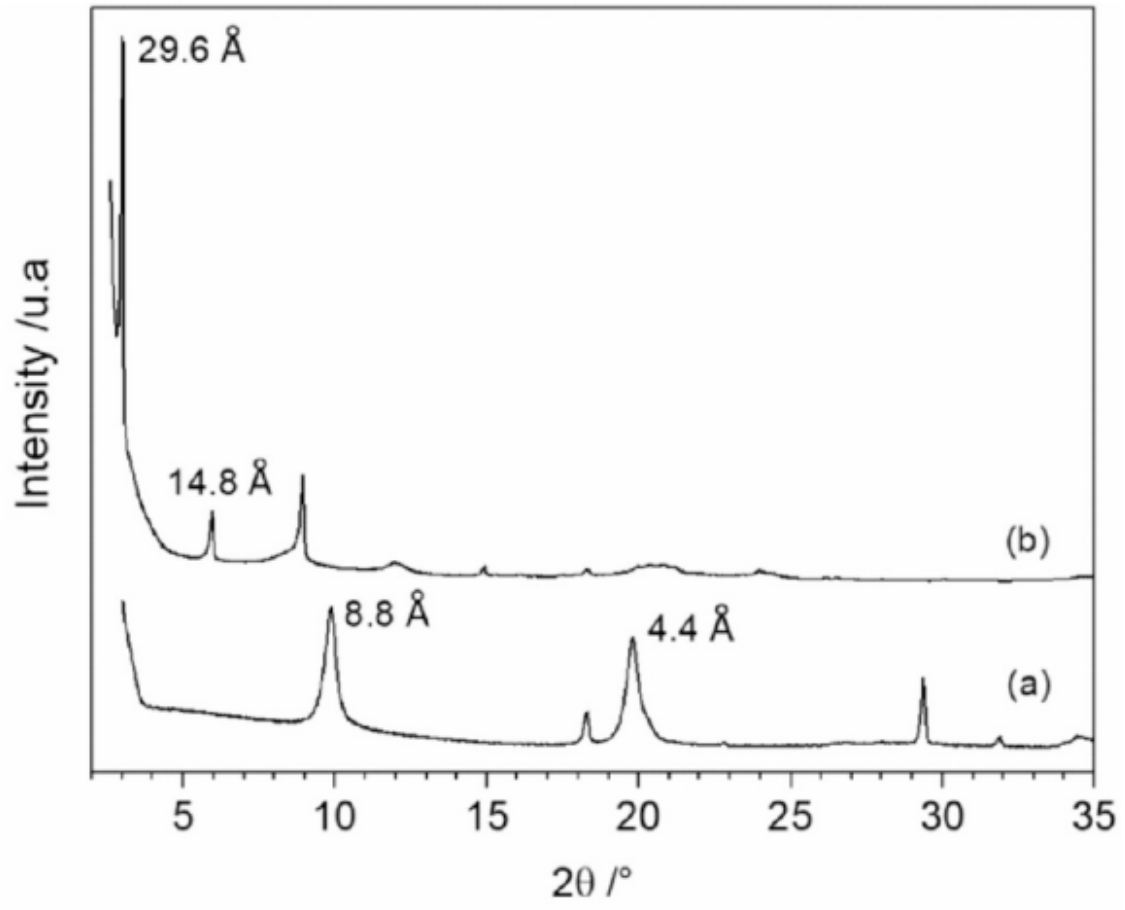

Fig. 2. Schematic arrangement of decanoate anions in the LDH spacing.

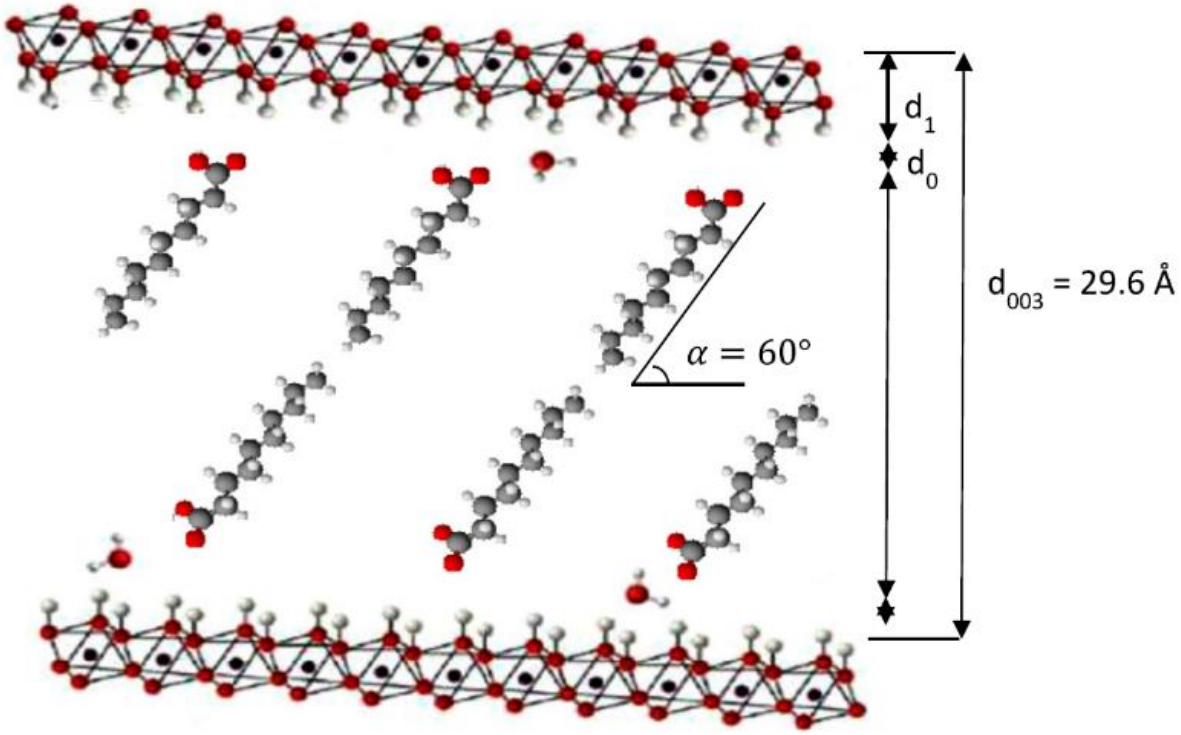

Fig. 3. DRIFTS spectra of (a) LDH-NO_3 and (b) LDH-C_{10}.

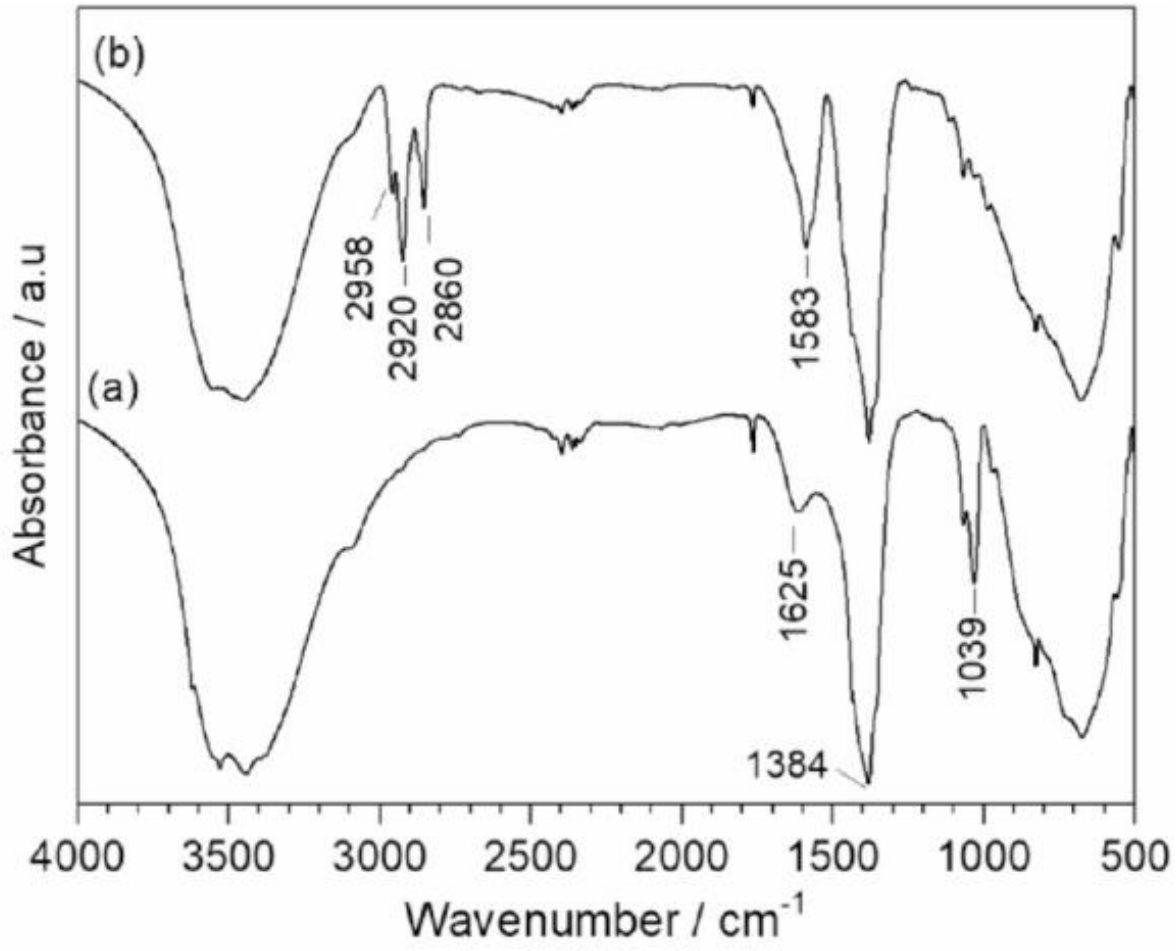

Fig. 4. Thermogravimetric measurements of (a) LDH-NO_3 and (b) LDH-C_{10} powder.

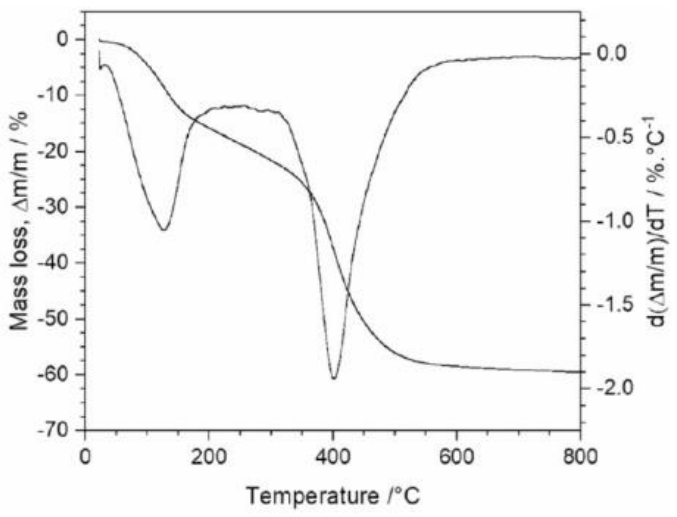

a)

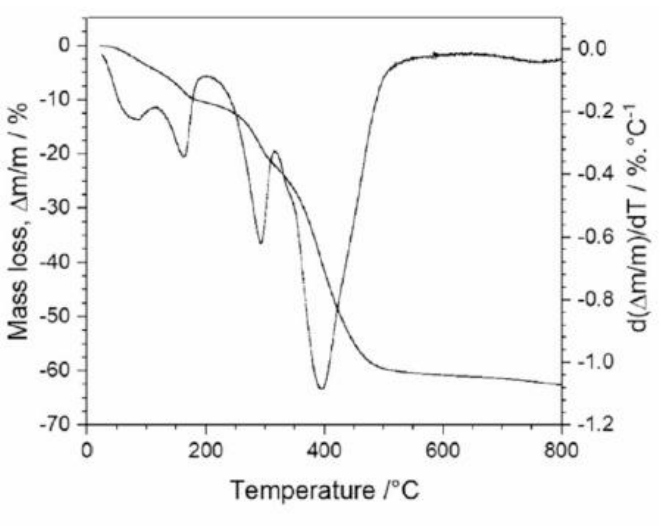

b)

Fig. 5. Typical SEM micrographs of LDH powders: (a) LDH-NO_3, (b) LDH-C_{10}.

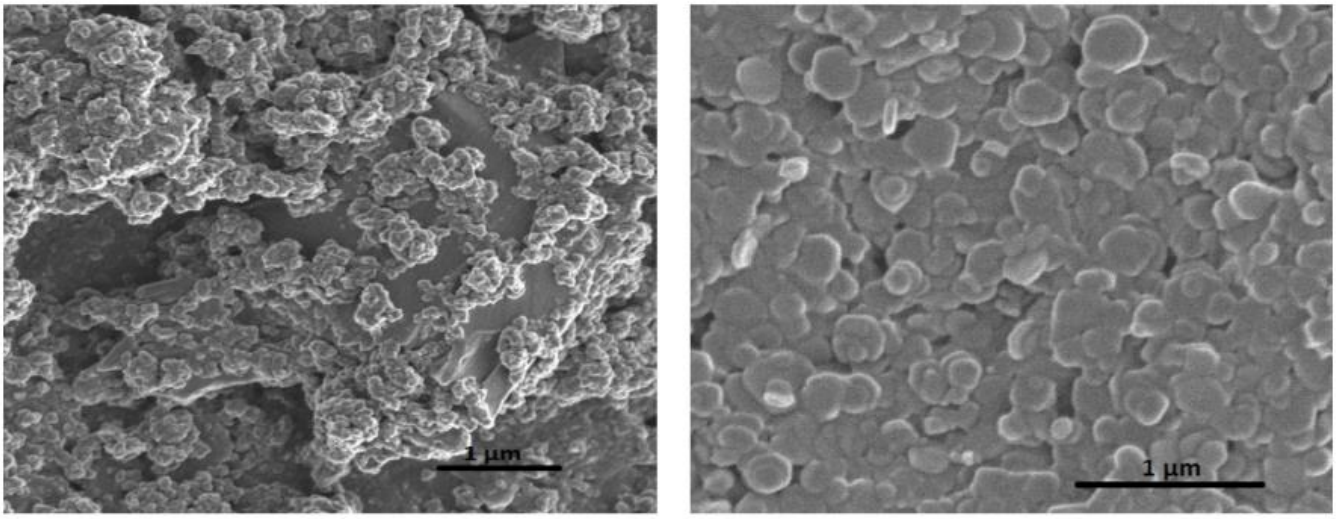

a) b)

Fig. 6. Impedance diagrams of mild steel after 20 h of immersion time in 0.1 M NaCl solution without and with pigments. (a) Bode-modulus and (b) Bode phase representation.

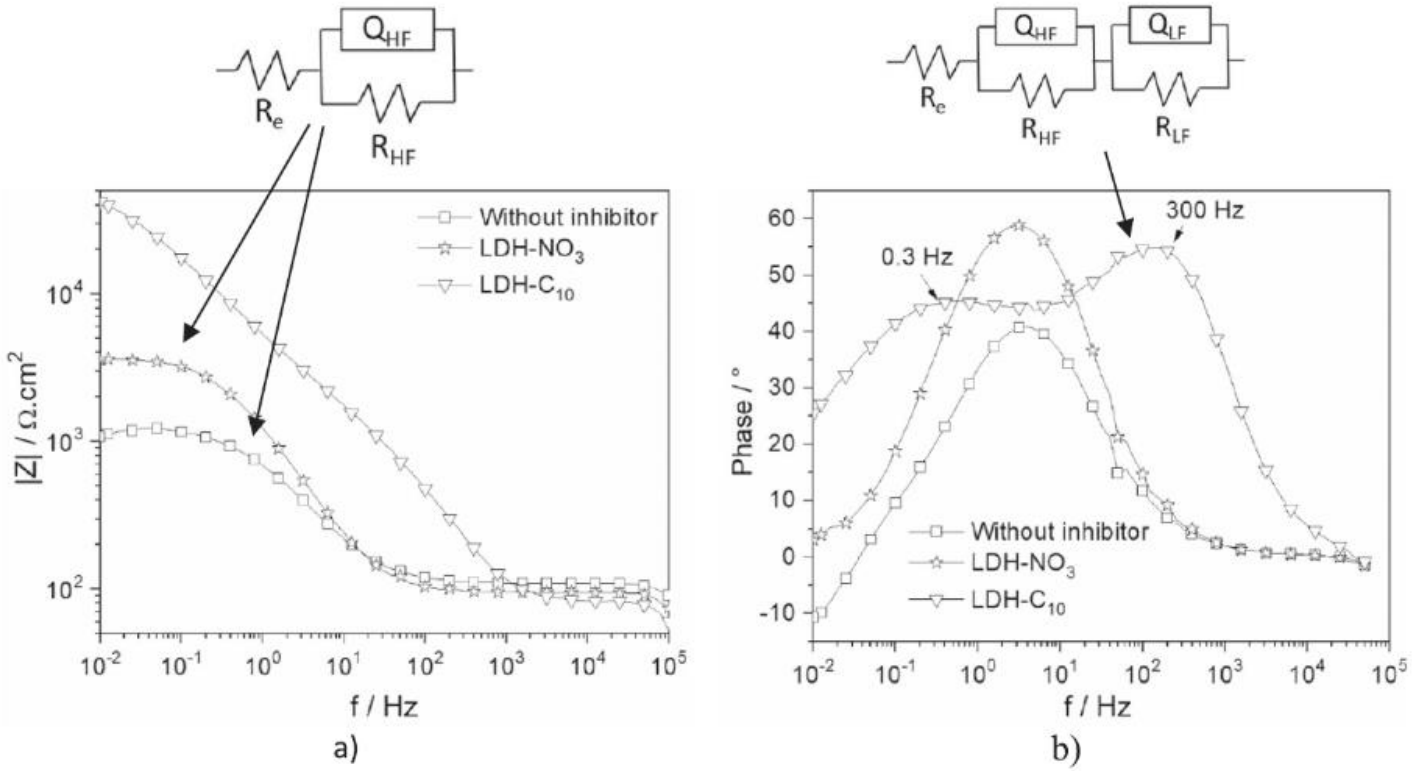

Fig. 7. Typical SEM micrographs taken on mild steel after 5 days of immersion in 0.1 M NaCl, (a) without pigments, (b) with LDH-NO_3 and (c) with LDH-C_{10}.

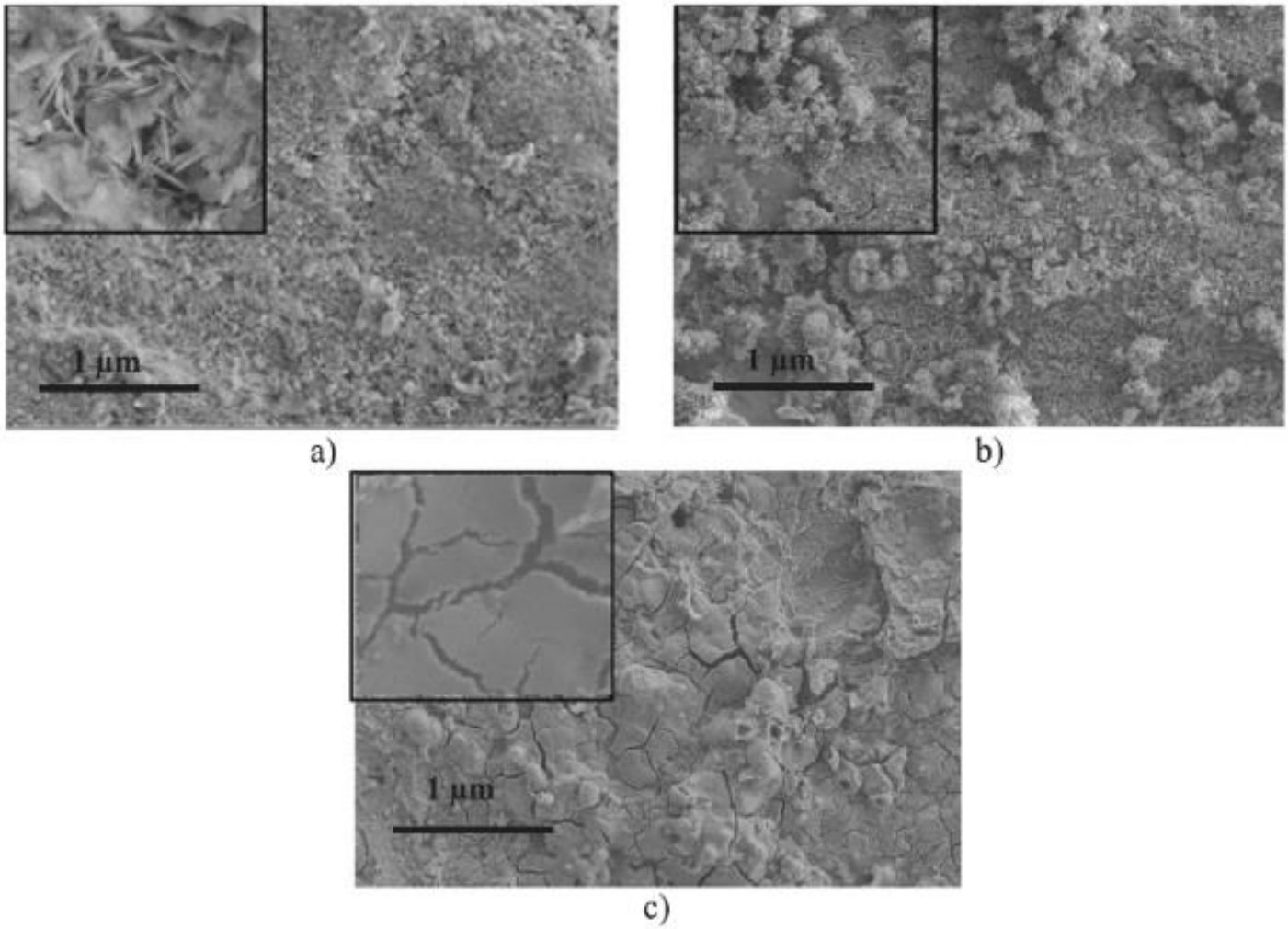

Fig. 8. Potentiodynamic curves with and without corrosion inhibitor pigments after 20 h of immersion time in 0.1 M NaCl.

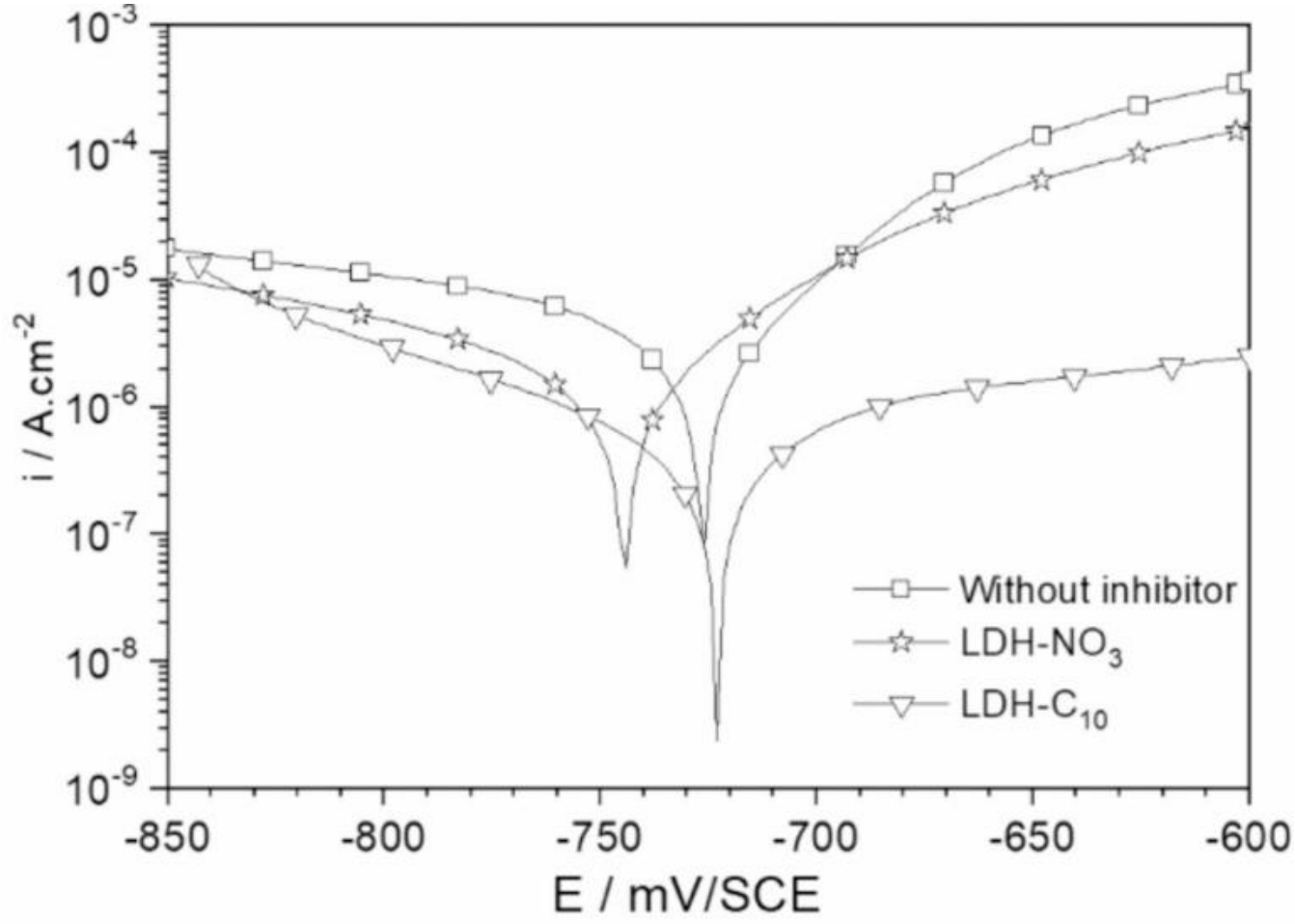

Fig. 9. Metallographic cross-section (SEM) of LDH-enriched alkyd resin coating on steel.

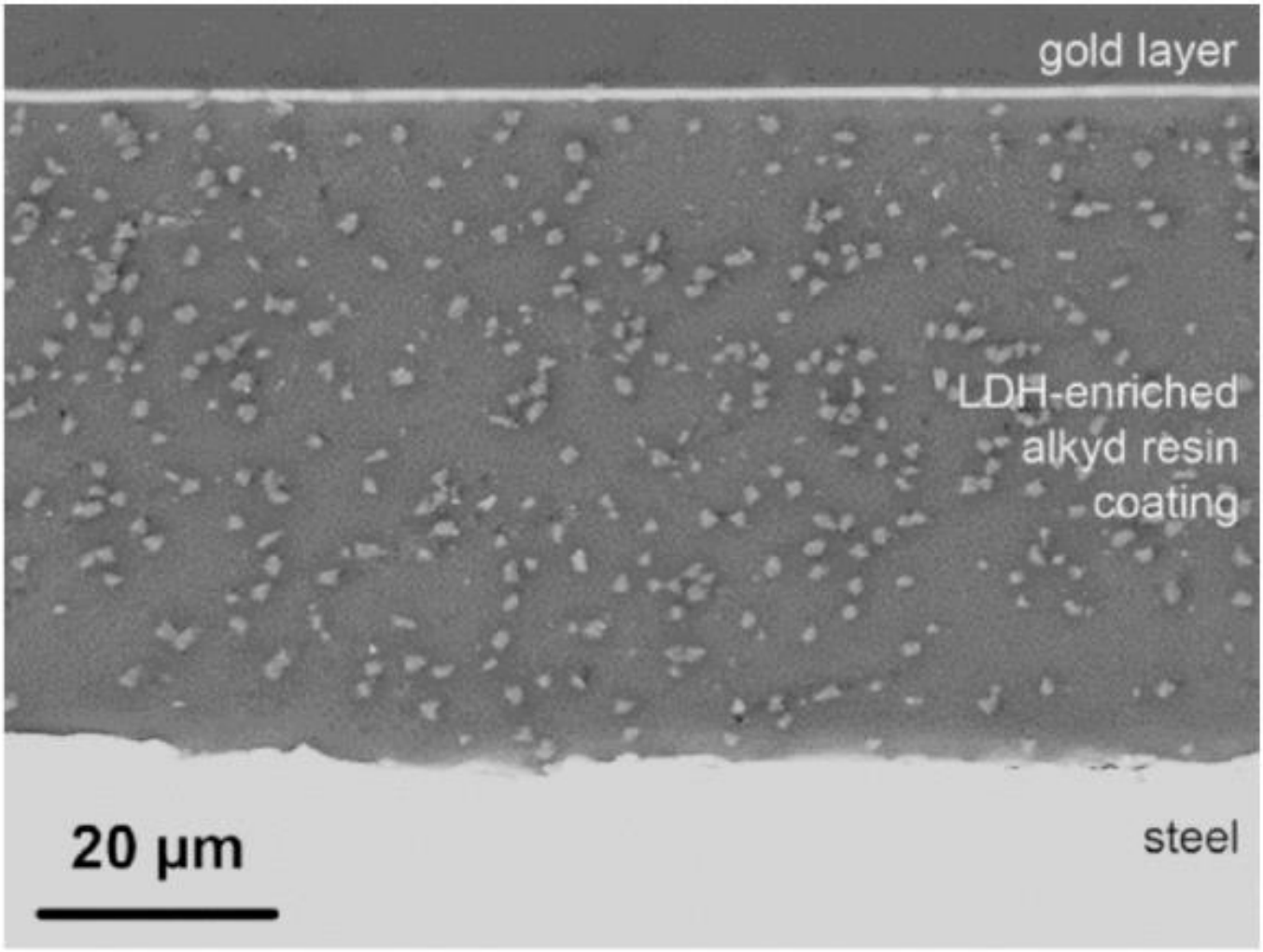

Fig. 10. Bode plot of coated steel in 3 wt% NaCl medium: (a) pure resin alkyd, (b) resin alkyd containing 5 wt% LDH-NO_3 and (c) resin alkyd containing 5 wt% LDH-C_{10}.

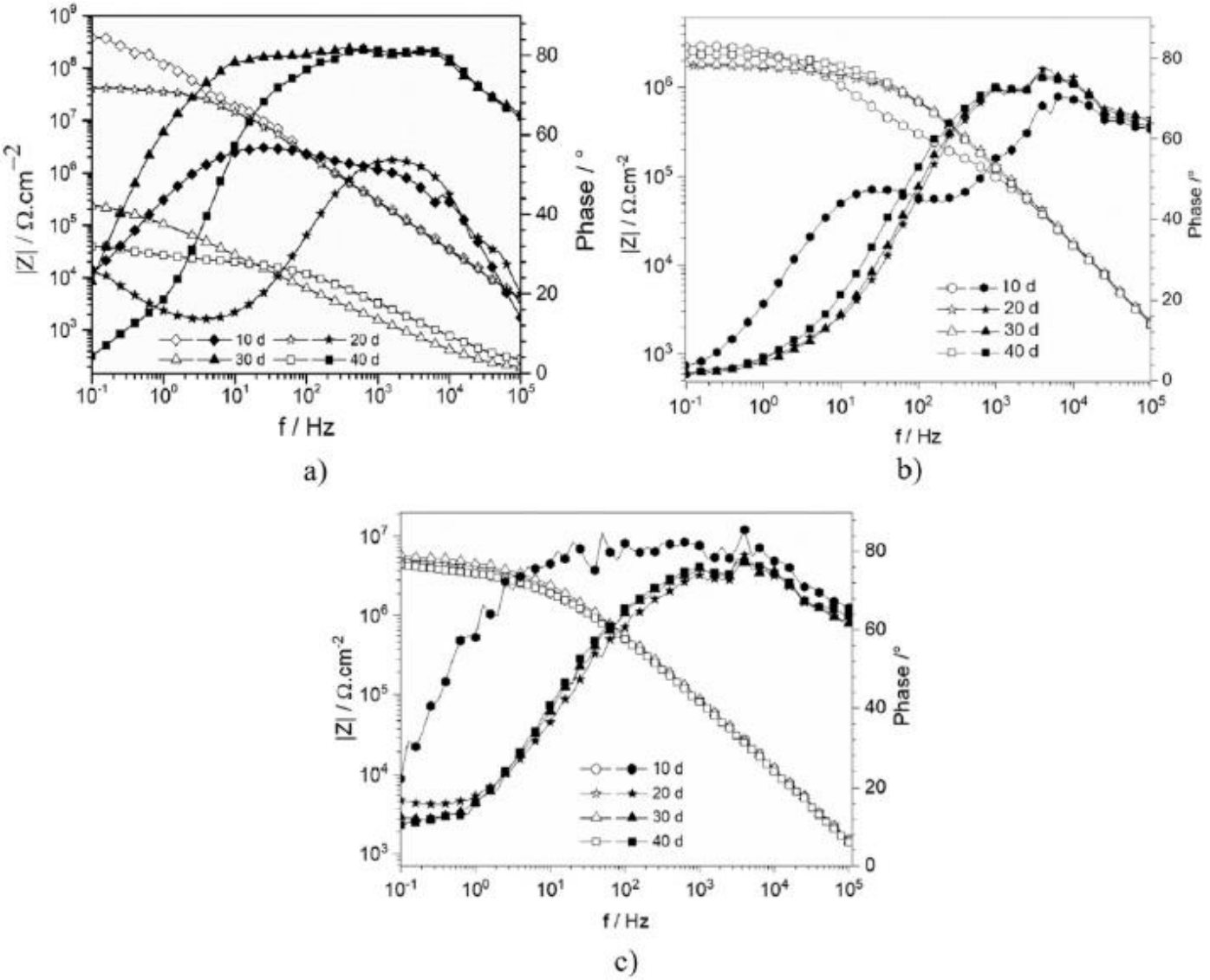

Fig. 11. |Z|10mHz versus immersion time in 3 %.wt NaCl solution for the steel coated with alkyd resin without and with 5 wt% LDH pigments.